# Effects of Width-to-Thickness Ratio of RHS Column on the Elasto-Plastic Behavior of Composite Beam

Eslami, Mohammadreza

Namba, Hisashi

Memoirs of the Graduate Schools of Engineering and System Informatics Kobe University
No. 6, pp. 1–6, 2014. doi:10.5047/gseku.e.2014.001

# Effects of Width-to-Thickness Ratio of RHS Column on the Elasto-Plastic Behavior of Composite Beam

Mohammadreza ESLAMI[1], Hisashi NAMBA[1]

[1]*Graduate School of Engineering, Department of Architecture*

(Received February 5, 2014; Accepted April 17, 2014; Online published May 13, 2014)

*Keywords:* *Composite Beam, Rectangular Hollow Section Column, Cyclic loading test, Rotation Capacity*

**The results of study on the elasto-plastic behavior of composite beam connected to Rectangular Hollow Section (RHS) column in the steel moment resisting frame buildings are presented in this paper. In order to investigate the effects of width-to-thickness (*B/t*) ratio of RHS column on the rotation capacity of composite beam, cyclic loading test were conducted on three full scale beam-to-column subassemblies. Detail study on the different steel beam damages and concrete slab damages are presented. It is found that occurrence of sever concrete bearing crush at the face of RHS column of specimen with smaller width-to-thickness ratio resulted to considerable reduction on the rate of strain increase in the lower flange. This behavior resulted to considerable improvement of rotation capacity in this specimen comparing with composite and even bare steel beam connected to the RHS column with larger width-to-thickness ratio.**

## 1. Introduction

Following to the 1995 Hyogo ken-Nanbu earthquake, fractures occurred in the beam-to-column connections of a number of steel moment frame buildings[1)]. According to post-earthquake observations in most cases fractures were happened at the bottom flanges and it is believed that composite action might be one of the reasons of such failure. Most of post-earthquake researches regarding the rotation capacity of beam were conducted on the bare steel beam specimens rather than composite specimens. According to past researches, it is already known that strain concentration at the lower flange affects the rotation capacity of composite beam. But the question arises that how strain is affected by different width-to-thickness ratios of RHS column and different slab compression forces, and how strain condition changes after the occurrence of damages in the concrete slab?

In the case of beam-to-RHS column connection, beam flanges are usually connected to column by through diaphragms, while beam web is connected to RHS column wall (flange) directly without any reinforcement. This might cause local out-of-plane deformation of column flange at the web connection. In this condition full capacity of beam web cannot be transmitted. This effect has been investigated for the bare steel beam[2)]. According to the research conducted by Okada et al.[3)], plastic rotation capacity of composite beam connected to RHS column decreased to almost half of bare steel beam. Further Research by Okada[4)] was conducted on the composite beams which were connected to the H-section (representing a RHS column which thickness of wall is infinite) and RHS columns with different width-to-thickness ratios of 24 and 38, and it was shown that significant reduction of composite beam rotation capacity will occur in the case of RHS column with large width-to-thickness ratios. Okada showed that out-of-plane deformation of RHS column is affected by reduction of web flexural capacity and movement of neutral axis toward beam top flange.

Matsuo[5)] conducted experimental test focusing on the rotation capacity of composite beam connected to the RHS column with width-to-thickness ratio of 29. According to that test results, rotation capacity of composite beam specimens were almost half of bare steel beam specimens. However, in current structural design, rotation capacity of composite beam is supposed to be equal to the bare steel beam.

This research is aiming to understand the mechanical mechanism of out-of-plane deformation of RHS column and its effect on the behavior of composite beam.

Actual behavior of composite beam connected to the RHS column with two different width-to-thickness ratios are studied through experimental tests. Results of different strength, stiffness and rotation capacity of beams are discussed through the study on the different damages in the steel beams and concrete slabs. Contribution of concrete slab on the condition of strain is investigated and strain studies before and after concrete crush were carried out to investigate the effects of lower flange strain on the rotation capacity of composite beam.

## 2. Experimental Test Specification

### 2.1 Test Specimens

In order to investigate the effects of RHS column width-to-thickness ratio on the rotation capacity of composite beam, cyclic loading test using T-shaped subassembly were conducted on three subassemblies of H-Beam(500×200×10×16) connected to RHS column with two different width-to-thickness ratios of 29 and 22 (□-350×350×12 & □-350×350×16). These two ratios were decided based on the common sections which are used in the actual construction of mid-rise buildings. As shown in Table 1, one bare steel beam specimen and two composite beam specimens were prepared. Figure 1 illustrates the configuration of specimens, test setups, weld joint details and steel deck geometry, respectively.

Table 1 Specimens Specification

| Specimen | Concrete Slab | RHS Column width-to-thickness *(B/t)* ratio |
|---|---|---|
| BS-29 | Not | 29 |
| CB-29 | Existed | 29 |
| CB-22 | Existed | 22 |
| Beam: H-500×200×10×16 | | Column: □-350×350×t |

As shown in the Figure, concrete slab with width of 1500 mm and thickness of 80 mm were used for composite beam specimens. In these specimens, deck plate type QL 99-50-12 applied and two stud bolts of ϕ16 were welded to the beam flange with pitch distance of 300 mm. Transverse distance between studs were considered as 80 mm. The number of shear studs is common to all specimens.

### 2.2 Weld Joint details

Weld Joint detail for beam-to-RHS column connection is illustrated in Figure 1(c). Beam flanges are connected to the column by "through diaphragm" to achieve smooth stress transfer from beam flange to the column, and preventing local deformation of RHS column wall. Beam web is connected to the wall of RHS column without reinforcement, and fillet welds were applied in both sides of the beam. This detail is common in Japan and it is recommended in JASS 6 2007 as an effective method. In all specimens shop welded joint type used by complete joint penetration (CJP) groove welds. $CO_2$ gas shielded metal arc welding method (GMAW) using YGW11 electrodes was conducted. Ceramic run of tabs were used and backing bars left in place. The weld access hole which is known as "scallop", was consisted of two arcs with radiuses of 35 and 10 millimetres, which is corresponded to post Hyogo ken-Nanbu earthquake scallop geometry type.

### 2.3 Material properties

The material utilized for the specimens were hot rolled sections with steel grade of SM490A and cold formed BCR295 for beams and columns, respectively. Diaphragm plates material were used with steel grade SN 490B. Actual material properties obtained by tensile coupon tests are reported in Table 2.

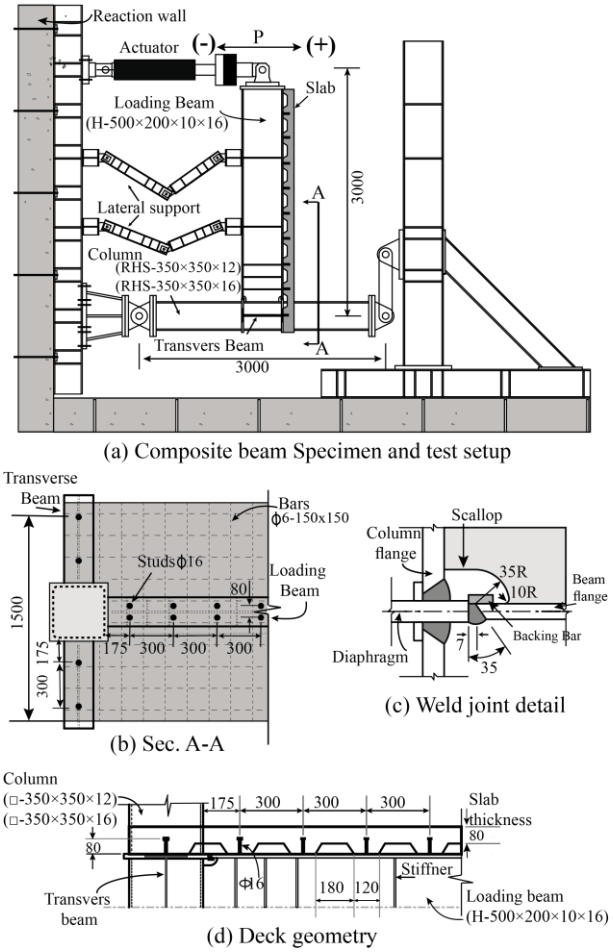


**Fig. 1** Configuration of specimens and test setups

Table 2 Material Properties

| Member | | Material Grade | $\sigma_y$ (N/mm$^2$) | $\sigma_u$ (N/mm$^2$) | YR= $\sigma_y/\sigma_u$ | EL (%) |
|---|---|---|---|---|---|---|
| Beam | Flange | SM490A | 383 | 551 | 69.5 | 40.6 |
| | Web | | 422 | 541 | 78.1 | 36.6 |
| RHS Column | CB-29 | BCR295 | 328 | 425 | 77.0 | 48.9 |
| | CB-22 | | 369 | 471 | 78.3 | 43.4 |
| Diaphragm | | SN490B | 370 | 531 | 69.7 | 49.9 |
| Weld Metal | | YGW11 | 420 | 536 | 78.3 | 31.4 |

Table 3 Shear Stud Push out Test Results

| Elastic Stiffness (KN/mm) | Shear Strength $q_y$ (KN) | Ultimate Shear Strength $q_{max}$ (KN) | $\delta_{max}$ (mm) |
|---|---|---|---|
| 346.9 | 65.5 | 88.9 | 2.36 |

Regarding the beam material toughness, Figure 2(a) plots the values of material Charpy V-Notch (CVN) impact test results associated with "fillet" area, which obtained from coupon tests. Fillet area is defined as the meeting point between the web and the flange which is illustrated in Figure 2 (b).

Studs material were used with steel grade JIS B1198-1995, and push-out tests were also carried out for the purpose of evaluating the shear strength and elastic stiffness of shear studs, summarized in Table 3.

The design strength of concrete used for composite beam specimens was 21.0 N/mm$^2$. The average concrete strength from cylinder tests was 28.4 N/mm$^2$ .

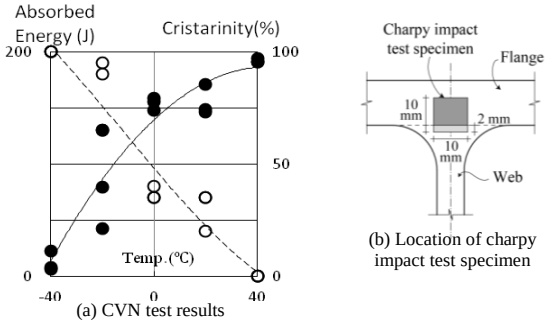


**Fig. 2** Charpy V-Notch impact test results for "fillet" area of beam

### 2.4 Test Procedure

As shown in Fig. 1, specimens were simply supported at both ends of column and the lateral load was applied at the top of beam. The cyclic loading program was applied, so the drift of the tip of beam increases as the loading cycle advances. The test protocol for this cyclic reverse loading is shown in Figure 3 which is consisted of one cycle of ±0.5 $\theta_p$ , 2 cycles in each ±2.0 $\theta_p$ , ±4.0 $\theta_p$ and other cycles in ±6.0 $\theta_p$ until the failure.

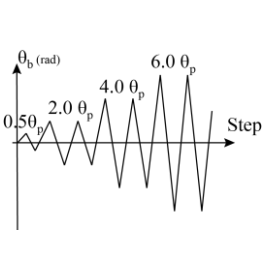


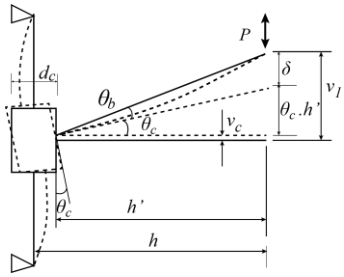


**Fig. 3** Cyclic loading protocol **Fig. 4** Definition of beam rotation

$\theta_p$ is the rotation corresponding to plastic moment capacity of bare steel beam ($M_p$), which is obtained by dividing beam's

plastic moment by its initial stiffness. $\theta_b$ is the beam rotation angle based on definition presented in Figure 4. Failure was defined as the fracture occurrence or 10% degradation from actual maximum strength obtained during the loading test.

## 3. Test Results

### 3.1. $M_b$- $\theta_b$ Hysteresis Diagrams

$M_b$-$\theta_b$ hysteresis graphs are shown in Figure 5 . In these graphs $M_b$ represents beam moment at column face and $\theta_b$ is beam rotation angle. It was observed that in the specimen which was connected to the RHS column with large width-to-thickness ratio of 29 (CB-29) rotation angle of composite beam reached to 2.0 $\theta_p$ , while bare steel beam specimen with same width-to-thickness ratio (BS-29) reached to second cycle of 4.0$\theta_p$. In the composite specimen which was connected to the smaller width-to-thickness ratio column (CB-22), considerable improvement of beam rotation capacity was observed and beam rotation angle could reach to 6.0 $\theta_p$. However, local buckling occurred in the beam lower flange of this specimen.

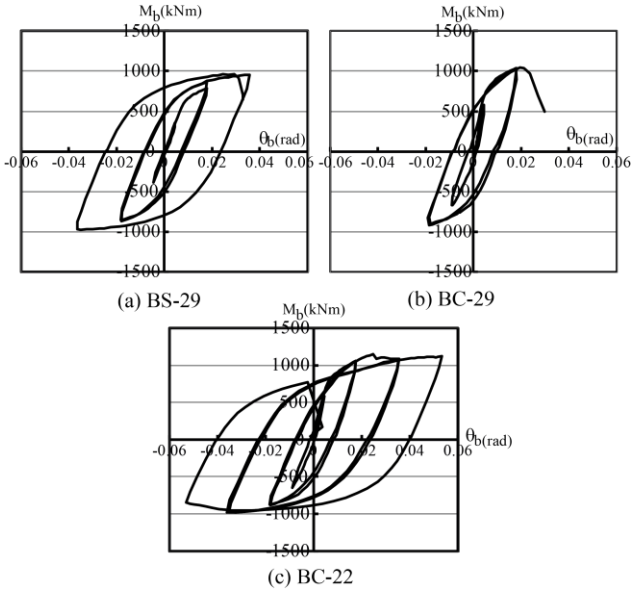


**Figure 5:** $M_b$- $\theta_b$ Hysteresis graphs

### 3.2. Steel Beam Damage Observations

3.2.1. Crack Initiation and progress

In all specimens, regardless of width-to-thickness ratio and existence of slab, crack initiation happened at the root of weld access hole. But in the composite specimen with large width-to-thickness ratio of 29 (CB-29) this crack occurred in the considerable early cycle of loading, which was second cycle of +2.0 $\theta_p$. While in the composite specimen with smaller width-to-thickness ration of 22 (CB-22) this crack occurred in the later stage of loading, which was second cycle of +4.0 $\theta_p$. Stage of loading which the crack initiated in the bare steel beam specimen (BS-29) was first cycle of +4.0 $\theta_p$ , which was later than CB-29 and earlier than CB-22. Crack initiation was defined when 0.2 mm crack was observed using crack scale. In Figure 6 typical crack initiation and progress at the root of weld access hole is shown for all specimens in the first cycle of +4.0$\theta_p$. Figure 7 shows that in which loading cycle first crack initiation was observed.

3.2.2. Final Failure Mode

Final failure of all specimens was determined by progress of above mentioned crack at the root of scallop of beam lower flange, shown in Figure 8. These fractures reproduced the failure modes of connections in the 1995 Hyogo ken-Nambu earthquake. Final failure manner of all specimens, were determined by quite ductile manner.

(a) BS-29: Crack initiation at +3.0$\theta_p$ (b) CB-29: Crack progress with width of 0.9mm (c) CB-22: No crack

**Fig. 6** Typical crack initiation and progress at the root of weld access in the first cycle of +4.0$\theta_p$

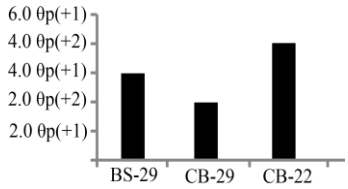


**Fig. 7** First crack initiation during loading test

**Fig.8** Typical final failure mode

### 3.3 Concrete slab damage observations

The concrete slabs were subjected to subsequent tensile and compressive load and the formation of cracks traced as loading progressed. In both composite specimens, three patterns of slab damage were observed during the test. “Longitudinal crack” which was parallel to the steel beam, “transverse crack” which formed perpendicular to the steel beam, and “bearing crush” which occurred due to direct compression and formed at the vicinity of RHS column face.

As shown in Figure 10 (a) and (b), in both width-to-thickness ratios of 29 and 22 specimens, comparable transverse cracks and longitudinal cracks occurred at similar cycle of loading which was first cycle -0.5 $\theta_p$ and +2.0 $\theta_p$ , respectively.

Initiation of bearing crush at the corners of RHS column were also happened at similar cycle of loading which was first cycle of +2.0 $\theta_p$ in both composite specimens, shown in Figure 11 and 12. However, in CB-29 specimen this damage did not progressed due to failure of specimen, while for the specimen with smaller width-to-thickness ratio (CB-22), by progress of loading cycles, sever concrete crush occurred at the vicinity of column face and over whole slab depth during the first cycle of +4.0 $\theta_p$, shown in Figure 13(b). This crush resulted to the sudden strength degradation which can be seen in the hysteresis diagram, shown in Figure 5(c) of sec. 3.1.

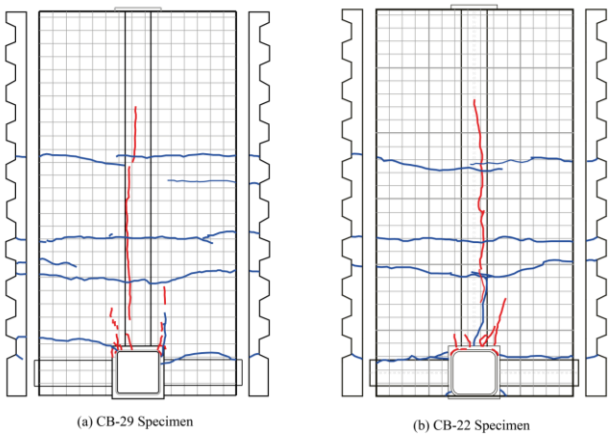


**Fig.10** Formation of longitudinal and transverse cracks until end of first cycle of +2.0 $\theta_p$

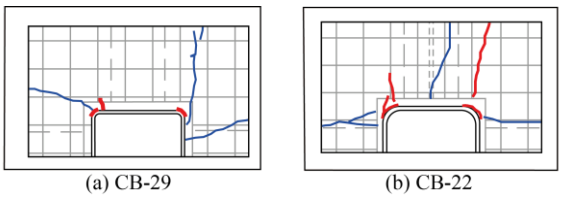


**Fig. 11** Initiation of bearing crush at corners of RHS column , comparable loading cycle +2.0 $\theta_p$(+1)

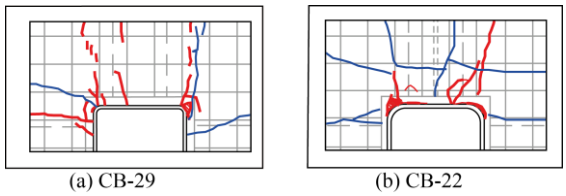


**Fig. 12** Comparable development of bearing crush until end of loading cycle +2.0 $\theta_p$(+2)

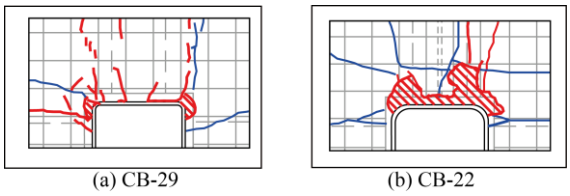


**Fig. 13** Final condition of concrete crush adjacent to the RHS column face

## 4. Effects of width-to-thickness ratio of RHS column

### 4.1. $M_b$-$\theta_b$ Skeleton curves

The skeleton curves obtained from $M_b$-$\theta_b$ hysteresis diagrams are plotted in Figures 14 (a) and (b). The method for plotting the skeleton curves, is shown in Figure 15(a) .

Figure 14(a) corresponds to skeleton curve obtained from positive loading, and Figure 14(b) corresponds to skeleton curve obtained from negative loading. In these graphs, actual plastic strength values are shown with solid circles, which are corresponding to one-sixth stiffness reduction, obtained by definition shown in Figure 15(b).

According to Figure 14, in positive flexure regardless of difference in column width-to-thickness ratio($B/t$), considerable increase in the elastic stiffness of composite specimens can be seen. The elastic stiffness of CB-29 and CB-22 are 1.93 and 1.83 times of bare steel beam, respectively. But in the case of negative flexure regardless of existence of slab, from the early stages of elastic region the stiffness is almost same.

Figures 16(a) and (b) illustrate the amount of elastic stiffness of specimens in the positive and negative flexure, respectively. In the figure, the amount of elastic stiffness in $\pm 0.5\theta_p$ and $\pm 2.0\ \theta_p$ (second cycle) are shown, and the calculated stiffness is plotted with horizontal dotted line. In $+0.5\theta_p$ positive flexure, considerable increase of stiffness in both composite specimens comparing with the bare steel beam specimen (BS-29) can be seen, But by progress of loading and development of damages in the concrete slab until $+2.0\ \theta_p$(+2), stiffness of both composite beam specimens reduced, and finally reached to almost bare steel beam stiffness.

As shown in Figure 16(b), in the negative flexure considerable difference for reduction of stiffness was not found between specimens. It can be explained that this behavior is resulted from removal of composite action in the negative flexure.

Regarding the actual plastic strength, from figure 15(a) it can be seen that in the positive flexure both composite specimens showed almost similar increase of plastic strength comparing with BS-29. The plastic strength of CB-29 and CB-22 are 1.27 and 1.31 times of bare steel beam, respectively. Also it is shown that in the bare steel beam specimen BS-29, after reaching to actual plastic strength, almost steady increase of strength can be seen until 0.05 rad. After reaching to this rotation angle, strength degradation happened due to development of crack in the root of weld access hole (scallop), which was explained in Sec. 2.3.2. In the case of composite beam specimens, it can be seen that both specimens showed similar behavior until 0.018 rad., but in CB-29 specimen degradation of strength gradually happened due to initiation and progress of crack at the root of lower flange weld access hole (scallop). On the other hand, in CB-22 specimen increase of strength continued by progress of loading until 0.025 rad . But sudden strength degradation can be seen in the skeleton curve of this specimen which was associated with concrete bearing crush at the vicinity of RHS column, which was discussed in sec. 2.3.3, and resulted to 5% strength reduction. After this drop in the strength, constant moment transmitted until 0.05 rad.

Figure 14 (b) shows that in the negative flexure, actual plastic strength of all specimens were comparable to the calculated plastic moment capacity of bare steel beam, which is plotted with dotted horizontal line in the figure.

Table 4 summarizes the results of observed ultimate strength of each specimen. Due to composite action, 8% increase in the ultimate flexural capacity of BC-29 observed comparing with bare steel beam specimen BS-29. Reduction of RHS column width-to-thickness ratio in CB-22 resulted to 10% increase in the ultimate strength of this specimen comparing with CB-29.

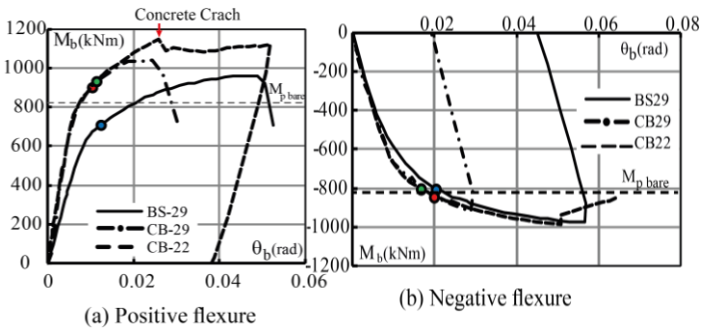


**Fig. 14** $M_b$-$\theta_b$ Skeleton curves

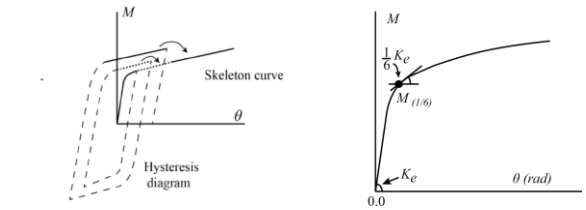


(a) Method for plotting the skeleton curve (b) Definition of strength

**Fig. 15** Method for plotting the skeleton curve and definition of actual plastic strength

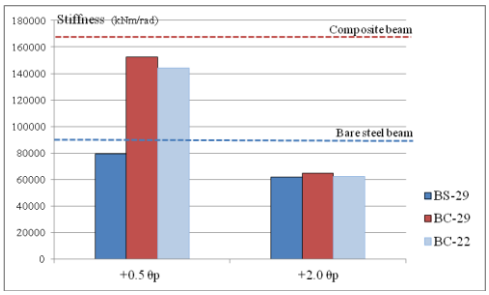


(a) Positive flexure

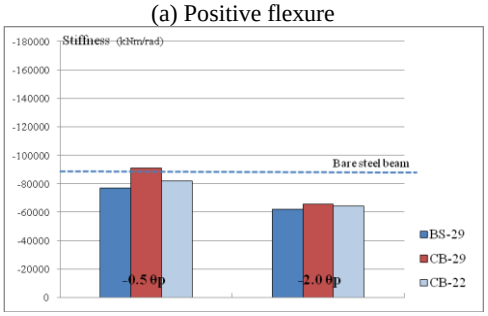


(b) Negative flexure

**Fig.16** Elastic stiffness of specimens

Table 4 Test results

| Specimen | Plastic Moment (kNm) | | Ultimate flexural Capacity (kNm) | |
|---|---|---|---|---|
| | $M_{p+}$ | $M_{p-}$ | $M_{max+}$ | $M_{max-}$ |
| BS-29 | 711 | 803 | 961 | 974 |
| CB-29 | 903 | 842 | 1042 | 922 |
| CB-22 | 934 | 801 | 1145 | 986 |

### 4.2. Strain Behavior

Figure 17 depicts the strain distribution across the length of beams upper and lower flange in the first cycle of +2.0 $\theta_p$ . Horizontal axis is the length and vertical axis is the amount of strain, measured by gauges attached at the 30 mm position from column face. As shown in Figure 18(a),(b) and (c) in each specimen, strain of flanges was measured by the strain gauges which were mounted on the steel sections. Strain gauges were attached to the inside of upper flange and both sides of lower flange.

According to Figure 17(a), it is found that the strain on the upper flange of both composite specimens remained almost zero, while in the bare steel beam specimen BS-29, upper flange strain amount reached to 2.7% negative strain. This behavior is resulted from existence of slab, which provides constraint condition for the upper flange of composite specimens.

Furthermore, for the lower flange it can be seen that flanges were subjected to positive strain. In both sides of lower flange of composite beam which was connected to the RHS column with large width-to-thickness ratio of 29 (CB-29 specimen), amount of strain is 2.2 times of bare steel beam specimen with same width-to-thickness ratio (BS-29). The amount of strain inside the lower flange is higher than outside, in the center of flange. By reduction of RHS column width-to-thickness ratio in CB-22 specimen, 55% reduction of strain comparing to CB-29 can be seen in both sides of flange. The amount of strain in CB-22 is just 1.2 times more than bare steel beam BS-29.

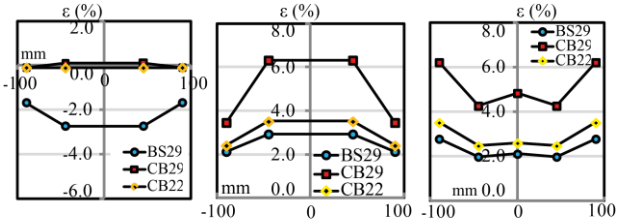


(a) upper flange inside (b) Lower flange inside (c) Lower flange outside

**Fig. 17** Strain distribution across the length of beams flange

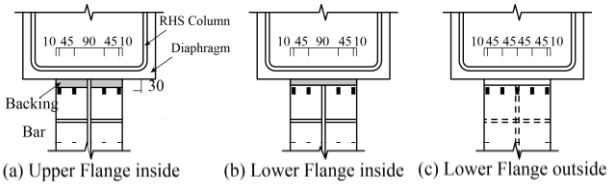


(a) Upper Flange inside (b) Lower Flange inside (c) Lower Flange outside

**Fig. 18** Strain gauges arrangement on the steel beam

The above strain condition is associated with the specific loading cycle of +2.0 $\theta_p$.The strain versus beam rotation angle is illustrated in Figure 19. It is shown that during the entire loading stages, for all specimens regardless of existence of slab or difference of width-to-thickness ratios, by the progress of loading and increase of beam rotation angle, the amount of strain in the flanges increased. But upper flange of composite specimens sustained considerable smaller amount of strain comparing to bare steel beam specimen BS-29. On the other hand for the lower flanges, although in the bare specimen BS-29 the strain condition was comparable with its upper flange, but considerable increase of strain happened in both composite specimens BC-29 and BC-22.

It is also found that in the composite beam specimen with smaller width-to-thickness ratio CB-22, after the beam rotation angle reached to 0.025 rad and sever concrete crush occurred, sudden reduction in the slope of strain curve happened in the lower flange. At the same time, slope of strain curve in the upper flange increased. This behavior can be explained that following to sever concrete bearing crush in CB-22, reduction of upper flange constraint condition occurred, and this resulted to change in the slope of strain curves of flanges.

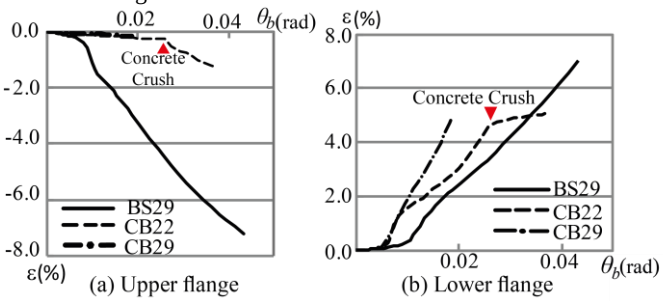


**Fig. 19** Strain versus beam rotation $\theta_b$

According to strain behavior study and damage observations which were explained in sec. 2.3.2, it is found that strain condition of lower flange affected the crack growth and progress in each specimen, and finally this resulted to different rotation capacity of beams. In CB-29 specimen, higher amount of strain resulted to earlier initiation and faster progress of crack comparing to bare steel beam BS-29. In CB-22 specimen, despite the higher amount of lower flange strain comparing with BS-29, but after the occurrence of concrete bearing crash, reduction of strain in the lower flange resulted to later initiation of crack at the root of weld access hole.

Figure 20 depict the crack growth in each specimen. Crack growth was investigated by plotting the measured crack opening ($\delta_{cr}$) versus beam rotation. In this figure, $\eta$ is the beam cumulative plastic rotation based on the definition shown on Figure 21. Table 5 summarizes the results of cumulative rotation capacity of each specimen. Smaller amount of strain on the lower flange of CB-22 resulted to later crack initiation, slower development and finally higher beam rotation capacity.

Figure 22 illustrates the beam cumulative plastic rotation ($\eta$) versus connection factor ($\alpha$) for this experimental test and also for specimens of Ref.(5) experimental test results. Connection factor ($\alpha$) is based on bare steel beam. In this figure, black is representing the results of composite specimens and white is representing the results of bare steel beam specimens. Triangle is associated with Ref.(5) specimens and circle is associated with of this test specimens. Due to difference in materials between this test and Ref.(5) test (SN400B), higher cumulative rotation capacity can be seen in the specimens of Matsuo's experimental test, but it can be seen that in both tests for same connection factor ($\alpha$) cumulative rotation of composite beam is reduced to almost less than half of bare steel beam.

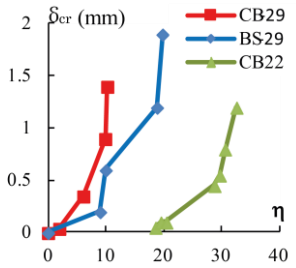


**Fig. 20** Crack growth

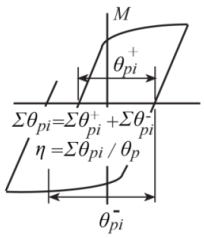


**Fig. 21** Definition of "$\eta$"

Table 5 Cumulative rotation capacity

| Specimen | $\eta$ |
|---|---|
| BS-29 | 20.4 |
| CB-29 | 10.7 |
| CB-22 | 45.3 |

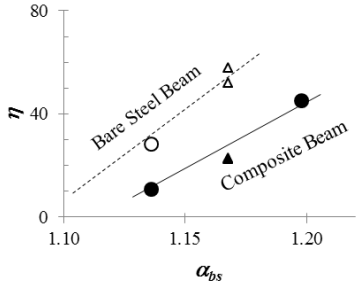


**Fig. 22** Cumulative rotation capacity ($\eta$) versus connection factor ($\alpha$) for this test and Ref.(5) specimens

## 5. Conclusions

This study was performed through the experimental tests on three full scale subassemblies to investigate the elasto-plastic behavior of composite beam connected to RHS columns with different *B/t* ratios. The following conclusions are made:

- Test showed that reduction of RHS column *B/t* ratio in composite specimens, did not result to considerable difference in the elastic stiffness and actual plastic strength in positive flexure, but considerable improvement in the cumulative rotation capacity was observed.
- Experimental test results revealed another specific difference between composite specimens. It was observed that in the specimen with smaller *B/t* ratio severe concrete bearing crush at the vicinity of column face resulted to the reduction in the rate of strain increase of lower flange. This resulted to significant effect in the improvement of rotation capacity.
- Occurrence of concrete crush can be considered as the start of removal of composite action effect and start of closing to the bare steel beam condition.
- This test reconfirmed the results of investigation in Ref. (5) for composite beams connected to RHS column with large *B/t* ratio of 29. According to considerable reduction of rotation capacity and in order to prohibit strain concentration on the lower flange, it is recommended to avoid composite action in this *B/t* ratio. Application of slit between the column face and concrete slab is recommended.
- Considering the significant effect of concrete crush on the strain behavior, further investigation is needed to clarify the mechanism of stress transfer, which FEA study will be conducted in the next part of this research. Also the behavior of composite beam with slit will be studied in the next part of this research.

## Acknowledgement

The research presented in this paper was supported by funds from Ministry of Education of Japan which is truly acknowledged.

## References

1) AIJ 1995d ; "Performance of Steel Buildings During the 1995 Hyogo ken-Nanbu Earthquake", *Architectural Institute of Japan(AIJ), Japan , Tokyo* (1995)
2) Recommendation for Design of Connections in Steel Structures, AIJ, pp. 144-150 , *Japan* (2012)
3) Okada, k. and S. Yamada; "Experimental Study on Deformation Capacity of Composite Beams With Conventional Type Beam-to-Column Connections", *J. Struct. Constr. Eng. ,AIJ*, No. 547, pp. 161–168, *Japan* (September 2001)
4) Okada, K., T. Sang-Hoon and S. Yamada; "Tests On Ductility Capacity of Composite Beams," *Proceedings of 7th Pacific Structural Steel Conference (PSSC)., USA* (2004)
5) Matsuo, A., Y. Nakamura; "A Study on Strain and Plastic Deformation Capacity of Composite Beam-to-RHS Column with Thorough Diaphragm ( Part1: Experimental Planning and Result)," *Proceedings of Annual Meeting of Architectural Institute of Japan(AIJ)*, pp. 535–536, *Japan* (September 1999)
6) Tanaka, T., K. Suita and N. Asakura; "Cyclic Loading Tests on Composite Beams with Scallops (Part 15) ," *Proceedings of Annual Meeting of Architectural Institute of Japan(AIJ)*, pp. 745–746, *Japan* (2013)